Published for SISSA by Springer

Received: December 3, 2024
Revised: February 11, 2025
Accepted: March 11, 2025
Published: April 9, 2025

Probing anomalous Higgs boson couplings in Higgs plus jet production at NLO QCD with full m_t-dependence

Benjamin Campillo Aveleira, Gudrun Heinrich, Matthias Kerner and Lucas Kunz

Institute for Theoretical Physics, Karlsruhe Institute of Technology, Wolfgang-Gaede-Str. 1, 76131 Karlsruhe, Germany

E-mail: benjamin.campillo@kit.edu, gudrun.heinrich@kit.edu, matthias.kerner@kit.edu, lucas.kunz@partner.kit.edu

Abstract: We present NLO QCD results for Higgs boson production in association with one jet, including anomalous Higgs-top and effective Higgs-gluon couplings within non-linear Effective Field Theory (HEFT), as well as the full top quark mass dependence. We provide differential results for the Higgs boson transverse momentum spectrum at $\sqrt{s} = 13.6\,\text{TeV}$ and discuss the effects of the anomalous couplings.

Keywords: Higgs Production, Anomalous Higgs Couplings, Higgs Properties, Higher-Order Perturbative Calculations

ArXiv ePrint: 2409.05728

Open Access, © The Authors.
Article funded by SCOAP^3.

https://doi.org/10.1007/JHEP04(2025)060

JHEP04(2025)060

Contents

1 Introduction **1**

2 Description of the method **3**
2.1 Framework of the calculation 3
2.2 Technical details 4

3 Numerical results and discussion of anomalous couplings **8**
3.1 Total cross sections and heat maps 8
3.2 Higgs boson transverse momentum distributions 11

4 Conclusions **13**

A Coefficients of coupling structures **14**

1 Introduction

Run 2 of the LHC was very successful in establishing the Higgs boson couplings to vector bosons and heavy fermions. With Run 3 and the high-luminosity upgrade the precision of the coupling measurements will further increase. Therefore it is important to have good control over the theoretical uncertainties, in particular to distinguish beyond the Standard Model (BSM) effects from effects due to insufficient higher order corrections.

It has been noticed some time ago [1–12] that the Higgs boson p_T-spectrum is an important observable to constrain both the Yukawa-couplings to top (and bottom) quarks as well as effective gluon-Higgs couplings due to interactions with unknown particles at higher scales, leading to operators that are not present in the Standard Model (SM). The impact of such effective operators on the $p_{T,H}$ spectrum in Higgs+jet production, including next-to-leading Order (NLO) QCD corrections in the heavy top limit (HTL), has been investigated in refs. [13–18], where the analysis of refs. [16–18] also includes investigations of effects due to the renormalisation group running of the Wilson coefficients.

In the SM, the leading order (LO) one-loop amplitude has been calculated in ref. [19], NLO results beyond the HTL were first obtained for the high transverse momentum region [11, 20]. The NLO result for general kinematics has first been obtained numerically [21–23], the top quark mass effects have been studied in detail in ref. [24]. Numerical results for the two-loop amplitude for Higgs plus jet production with full top quark mass dependence also have been calculated in ref. [25] in the framework of the full next-to-next-to-leading order (NNLO) corrections to inclusive Higgs production, a study of the Higgs boson transverse momentum spectrum through the combination of this calculation with a parton shower has been presented in ref. [26].

On the analytic side, compact analytic expressions for the one-loop amplitudes for Higgs + 4 parton scattering, providing an efficient way to calculate the NLO real radiation contributions, have been presented in ref. [27]. After the relevant two-loop master integrals have become available [28–30], the full NLO calculation based on analytic results for the

JHEP04(2025)060

two-loop integrals has been completed in ref. [31], including both top and bottom masses as well as a comparison of the on-shell and $\overline{\text{MS}}$ schemes to renormalise the top quark mass. Two-loop bottom quark mass effects also have been studied in ref. [32]. Mixed QCD-EW corrections have been presented in refs. [33–35], partial EW corrections are considered in refs. [36–38]. NNLO results for Higgs plus jet production in the HTL are available already since some time ago [39–45]. Higgs production in association with one or multiple high-energy jets is available within the `HEJ` framework [46, 47]. In ref. [48], light quark mediated Higgs boson production in association with a jet at NNLO and beyond is considered in the framework of resummation.

The Higgs boson transverse momentum spectrum for boosted Higgs bosons already has been used by the experimental collaborations to place limits on anomalous top-Higgs and gluon-Higgs couplings [49–53]. The latter can be parameterised by c_t and c_g in Higgs Effective Field Theory (HEFT), also called Electroweak Chiral Lagrangian [54–59]. These couplings also enter inclusive Higgs boson production in gluon fusion, which is known to agree with the SM prediction to a level approaching 5%. Therefore, these anomalous couplings are fairly well constrained already (also from other processes such as $t\bar{t}H$ production for the case of the Higgs-top coupling [60, 61]). However, it is well known that there is a degeneracy between c_t and c_g when considering only inclusive Higgs production, which is lifted when considering the p_T-spectrum of the Higgs boson at large transverse momenta [4, 5, 14, 15]. Up to now, the effects of these operators have not yet been studied in combination with NLO corrections to Higgs+jet production including the full top quark mass dependence. However, both the SM top quark mass effects as well as these anomalous couplings affect the tail of the $p_{T,H}$-distribution considerably. Therefore it is important to study in detail the interplay of both, higher order QCD corrections and potential effects of new physics in an EFT framework.

In this work we would like to address this point and investigate the effects of these anomalous couplings on the Higgs+jet cross section and transverse momentum distributions, based on a calculation of the full NLO QCD corrections in the SM [21]. Working in HEFT rather than Standard Model Effective Field Theory (SMEFT) [62–65], our power counting scheme is not based on canonical dimension counting, i.e. the counting of inverse powers of a new physics scale Λ, but instead on the counting of the chiral dimension d_χ, which is related to the (explicit or implicit) loop order L through $d_\chi = 2L + 2$. The chromomagnetic top-quark dipole operator has chiral dimension $d_\chi = 4$ and therefore is considered to be subleading, as explained in section 2. Thus the inclusion of chromomagnetic dipole operators will be considered in subsequent work, together with other subleading operators entering at the same level, such as four-fermion operators.

The structure of this paper is as follows: in section 2 we describe how the anomalous couplings relate to inclusive Higgs production and how they affect the large-p_T spectrum of the Higgs boson. We also give some technical details about the calculation. Section 3 is dedicated to the description of phenomenological results, providing heat maps that show the effects of the anomalous couplings on the total cross section and discussing the effect of some HEFT benchmark points on the Higgs boson transverse momentum spectrum, before we conclude in section 4.

JHEP04(2025)060

2 Description of the method

2.1 Framework of the calculation

We include anomalous couplings based on the effective Lagrangian

$$\mathcal{L} \supset -c_t\, m_t\, \frac{H}{v}\bar{t}t + \frac{\alpha_s}{8\pi} c_g \frac{H}{v} G^a_{\mu\nu} G^{a,\mu\nu}\,. \tag{2.1}$$

In the SM, $c_t = 1$ and $c_g = 0$. We assume that the anomalous couplings are induced by new physics interactions at a scale Λ considerably larger than the electroweak scale. While the process $pp \to H$+jet is loop induced in the SM, the second part of the Lagrangian now also introduces effective tree level interactions. The factor proportional to $\alpha_s/8\pi$ indicates that these interactions are stemming from loops of heavy particles that have been integrated out to arrive at the effective Higgs-gluon coupling. In the region $2m_t \lesssim \sqrt{\hat{s}} \lesssim \Lambda$ the top quark loops are resolved while the heavier particles in the loop generate the effective point-like Higgs-gluon interaction. The coefficient c_t is a modification factor of the top Yukawa coupling, which can arise for example by mixing with heavy top partners [4, 66]. The chromomagnetic top-quark dipole operator $\mathcal{O}_{tg} = y_t g_s \bar{t}_L \sigma^{\mu\nu} T^a G^a_{\mu\nu} (v + H) t_R$ can only be generated through contracted loops [65, 67, 68] in weakly coupled, renormalisable UV completions and we stick to such extensions of the SM. Therefore, inserting the operator into the one-loop diagrams that constitute the LO in the SM, the resulting diagrams are effectively of two-loop order (chiral dimension $d_\chi = 6$), thus coming with a loop suppression factor $\sim 1/(16\pi^2)$. The operator $\mathcal{O}_{hg}$, mediating direct Higgs-gluon couplings, also pertains to the class of loop-generated operators. However, insertions of $\mathcal{O}_{hg}$ enter at tree-level and therefore have chiral dimension $d_\chi = 4$. The SM NLO QCD corrections also lead to two-loop diagrams and therefore come with a loop factor $1/(16\pi^2)$ relative to the LO diagrams. However, the SM two-loop QCD diagrams come with an extra factor $g_s^2 = 4\pi\alpha_s$ relative to the Born diagrams, while the chromomagnetic dipole operator comes with an extra factor $y_t g_s$. As we only calculate the QCD corrections, which are of order $\mathcal{O}(\alpha_s)$ relative to the Born amplitude, we neglect the two-loop corrections stemming from the chromomagnetic top-quark dipole operator in the present work. This is in line with the procedure followed in ref. [69] for the QCD corrections to Higgs boson pair production. Furthermore, we do not include any 4-quark operators nor CP-violating operators.

The matrix element squared for each partonic subprocess can be written as [5]

$$|\mathcal{M}|^2 \propto |c_t\, \mathcal{M}_f(m_t) + \kappa_g\, \mathcal{M}_{Hg}(m_t)|^2, \tag{2.2}$$

where $\mathcal{M}_f$ denotes the parts of the amplitude where the Higgs boson couples to a top quark, and $\mathcal{M}_{Hg}$ the amplitude parts containing an effective point-like Higgs-gluon interaction. Note that the NLO amplitude can also contain both, a top quark loop and a point-like Higgs-gluon interaction. However, in these diagrams the top quarks couple only to gluons, with an SM coupling. We use $\kappa_g = \frac{3}{2} c_g$ such that the HTL corresponds to $\kappa_g \to 1$ and $c_t = 0$. The total cross section for $pp \to H + \text{jet}$ can be written as a quadratic polynomial in c_t and c_g, both at LO and at NLO.

Integrating over the jet momenta, the total inclusive cross section for Higgs boson production in gluon fusion should be retrieved. As is well known, due to the "Higgs Low

JHEP04(2025)060

Energy Theorem" [70–72], the total cross section for Higgs production in gluon fusion is rather insensitive to the masses of heavy particles circulating in the loop. This is also reflected in the fact that, at energy scales below $2m_t$, the inclusive Higgs production cross section is approximated very well by the HTL. An extra high-p_T jet can serve as a handle to resolve heavy quark loops, therefore new physics effects could show up in the tail of the Higgs p_T-distribution.

From the Lagrangian (2.1) one obtains for the inclusive Higgs production cross section at LO (see ref. [4]):

$$\frac{\sigma_{\text{incl}}(c_t, \kappa_g)}{\sigma_{\text{incl}}^{\text{SM}}} = (c_t + \kappa_g)^2 + \mathcal{O}\left(\frac{\kappa_g}{c_t + \kappa_g}\frac{m_H^2}{4m_t^2}\right). \tag{2.3}$$

As the measured total Higgs production cross section in gluon fusion agrees very well with the SM result, the relation $(c_t+\kappa_g)^2 = 1$ should be fulfilled to about 10% level, assuming that subleading operators do not have a drastic effect, which would lead to more freedom in the relation between c_t and κ_g. In the pure HTL, the proportionality of the cross section to $(c_t + \kappa_g)^2$ is fulfilled exactly, also for the NLO amplitudes, because there are no diagrams at NLO which contain both c_t and c_g simultaneously, such that the HTL of the full SM NLO amplitudes gives exactly the amplitudes proportional to κ_g. This degeneracy is broken in the Higgs boson transverse momentum spectrum because as $p_{T,H}$ increases, the top quark loops start to become resolved and therefore the kinematic behaviour of the contribution proportional to c_t is different from the one in the HTL for large values of $p_{T,H}$. On the other hand, as the differential cross section decreases rapidly with $p_{T,H}$, the effects of anomalous couplings on the total cross section should be small as long as the relation $(c_t + \kappa_g)^2 = 1$ is fulfilled. Therefore it is useful to consider the cross section for $pp \to H +$ jet as a function of the cut on $p_{T,H}$ [4, 5]:

$$\frac{\sigma_{Hj}(p_{T,H}^{\text{min}}, c_t, \kappa_g)}{\sigma_{Hj}^{\text{SM}}(p_{T,H}^{\text{min}})} = (c_t + \kappa_g)^2 + \delta_1(p_{T,H}^{\text{min}})\, c_t\, \kappa_g + \delta_2(p_{T,H}^{\text{min}})\, \kappa_g^2\,, \tag{2.4}$$

where the coefficients δ_i depend on the cut $p_{T,H}^{\text{min}}$. For small $p_{T,H}^{\text{min}}$ the coefficients δ_i at LO are very small, modifying the cross section in the permille to percent range below $p_{T,H} \sim 350$ GeV [4]. However, recent LHC measurements have reached transverse momentum regions beyond 600 GeV [49, 51, 53, 73]. Furthermore, the study of refs. [4, 5] was at LO only, and the one of refs. [13–15] is based on the HTL when going beyond LO. In section 3, we will investigate how the anomalous couplings modify the large-$p_{T,H}$ spectrum at NLO with full top quark mass dependence.

2.2 Technical details

The cross section for $pp \to H+$jet consists of $gg, qg, \bar{q}g$ and $q\bar{q}$ initiated subprocesses. The calculation largely relies on the corresponding setup for the SM case, described in ref. [21].

Leading order amplitudes. The LO amplitudes in the full theory as well as the amplitudes involving c_g were implemented analytically, relying on ref. [19], while the one-loop real radiation contribution and the two-loop virtual amplitudes rely on semi-numerical evaluations.

JHEP04(2025)060

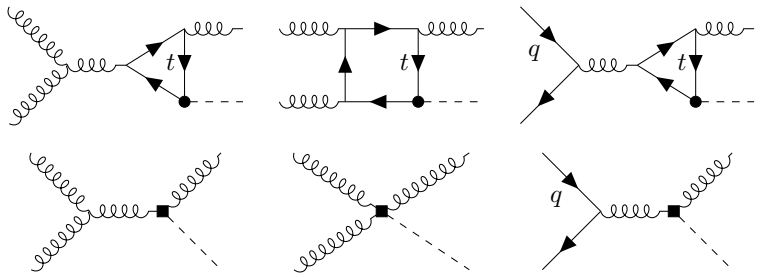

Figure 1. Example diagrams contributing to Higgs plus one jet production at LO, based on the chiral Lagrangian given in eq. (2.1).

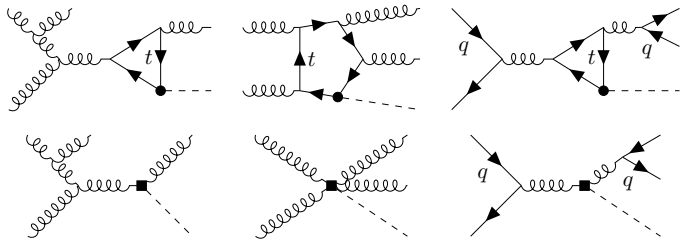

Figure 2. Examples for real radiation diagrams of order g_s^4.

As a cross-check we also generated the Born amplitudes with GoSam [74, 75] using the UFO [76, 77] model described in ref. [69], finding agreement between the two implementations at amplitude and cross section level. Example diagrams contributing at Born level are shown in figure 1.

Real radiation. The real radiation corrections contain one-loop diagrams up to pentagons as well as tree-level 5-point-diagrams, examples are shown in figure 2. The loop-induced real radiation matrix elements were implemented using the interface [78] between GoSam [74, 75] and the `POWHEG-BOX-V2` [79–81], modified accordingly to compute the real corrections based on one-loop amplitudes for the part of the amplitude that contains explicit top quark loops. The one-loop amplitudes were generated with GoSam-2.0 [75], that uses `Qgraf` [82], `FORM` [83] and `spinney` [84] for the generation of the Feynman diagrams, and offers a choice from `Samurai` [85, 86], `golem95C` [87–89] and `Ninja` [90] for the reduction, as well as `OneLOop` [91] or `QCDloop` [92] for the scalar integrals. At run time the amplitudes were computed using `Ninja` [90], `golem95C` [88] and `OneLOop` [91] for the evaluation of the one-loop integrals.

Virtual corrections. For the virtual two-loop amplitudes, we have used the results of the calculation presented in ref. [21], which is based on Reduze 2 [93] and SecDec-3 [94], which evolved to pySecDec [95–97]. Examples of virtual diagrams are shown in figure 3. The values for the Higgs boson and top quark masses have been set to $m_H = 125$ GeV and $m_t = 173.055$ GeV, which means $m_H^2/m_t^2 = 12/23$. Fixing these values reduces the number of independent scales in the two-loop amplitudes to two variables, the Mandelstam invariants $\hat{s}$ and $\hat{t}$.

The $gg \to g\,H$ amplitude can be decomposed into four tensor structures. After imposing parity conservation, transversality of the gluon polarization vectors and the Ward identity,

JHEP04(2025)060

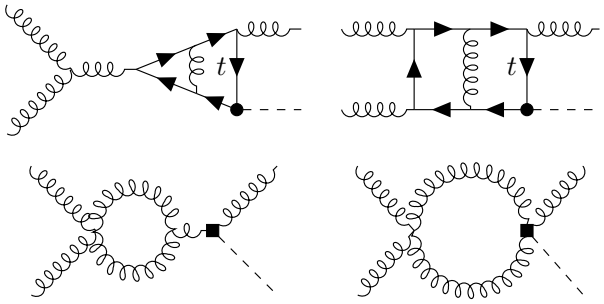

Figure 3. Examples for virtual diagrams of order g_s^5 in the gluon fusion channel.

the amplitude can be written as a linear combination of four form factors F_{ijk} multiplying the tensor structures $T_{ijk}^{\mu\nu\tau}$ [98]:

$$\mathcal{M}^{\mu\nu\tau} = F_{212}T_{212}^{\mu\nu\tau} + F_{332}T_{332}^{\mu\nu\tau} + F_{311}T_{311}^{\mu\nu\tau} + F_{312}T_{312}^{\mu\nu\tau}\,, \tag{2.5}$$

where

$$\begin{aligned}
T_{212}^{\mu\nu\tau} &= (s_{12}g^{\mu\nu} - 2p_2^\mu p_1^\nu)(s_{23}p_1^\tau - s_{13}p_2^\tau)/(2s_{13})\,,\\
T_{332}^{\mu\nu\tau} &= (s_{23}g^{\nu\tau} - 2p_3^\nu p_2^\tau)(s_{13}p_2^\mu - s_{12}p_3^\mu)/(2s_{12})\,,\\
T_{311}^{\mu\nu\tau} &= (s_{13}g^{\tau\mu} - 2p_1^\tau p_3^\mu)(s_{12}p_3^\nu - s_{23}p_1^\nu)/(2s_{23})\,,\\
T_{312}^{\mu\nu\tau} &= \Big(g^{\mu\nu}(s_{23}p_1^\tau - s_{13}p_2^\tau) + g^{\nu\tau}(s_{13}p_2^\mu - s_{12}p_3^\mu) + g^{\tau\mu}(s_{12}p_3^\nu - s_{23}p_1^\nu)\\
&\quad + 2p_3^\mu p_1^\nu p_2^\tau - 2p_2^\mu p_3^\nu p_1^\tau\Big)/2\,,
\end{aligned} \tag{2.6}$$

with $s_{ij} = (p_i + p_j)^2$. Three of the form factors are related by cyclic permutations of the external gluon momenta while the fourth is invariant under such permutations. The $q\bar{q} \to g\,H$ amplitude similarly can be decomposed in terms of two tensor structures as [99]:

$$M_\rho \epsilon^\rho = F_1 T_1 + F_2 T_2\,, \tag{2.7}$$

where

$$\begin{aligned}
T_1 &= \bar{u}(p_1)\ \not{p}_3\, v(p_2) p_2\ \cdot\ \epsilon_3 - \bar{u}(p_1)\ \not{\epsilon}_3\, v(p_2) p_2\ \cdot\ p_3\,,\\
T_2 &= \bar{u}(p_1)\ \not{p}_3\, v(p_2) p_1\ \cdot\ \epsilon_3 - \bar{u}(p_1)\ \not{\epsilon}_3\, v(p_2) p_1\ \cdot\ p_3\,.
\end{aligned} \tag{2.8}$$

In this case the form factors are related by interchanging the external quark and anti-quark momenta. The $qg \to q\,H$ amplitude can be obtained from the $q\bar{q} \to g\,H$ amplitude by crossing.

The form factors can be extracted introducing projectors $P_{ijk}^{\mu\nu\tau}$ satisfying $P_{ijk}^{\mu\nu\tau} M_{\mu\nu\tau} = F_{ijk}$. The four projectors for the $gg \to gH$ amplitude in D-dimensional space-time are:

$$\begin{aligned}
P_{212}^{\mu\nu\tau} &= \frac{1}{(D-3)s_{23}}\left(-\frac{Ds_{13}}{s_{12}^2 s_{23}}T_{212}^{\mu\nu\tau} - \frac{D-4}{s_{23}^2}T_{332}^{\mu\nu\tau} - \frac{D-4}{s_{12}s_{13}}T_{311}^{\mu\nu\tau} + \frac{D-2}{s_{12}s_{23}}T_{312}^{\mu\nu\tau}\right)\,,\\
P_{332}^{\mu\nu\tau} &= \frac{1}{(D-3)s_{12}}\left(-\frac{D-4}{s_{12}s_{23}}T_{212}^{\mu\nu\tau} - \frac{Ds_{12}}{s_{13}s_{23}^2}T_{332}^{\mu\nu\tau} - \frac{D-4}{s_{13}^2}T_{311}^{\mu\nu\tau} + \frac{D-2}{s_{13}s_{23}}T_{312}^{\mu\nu\tau}\right)\,,\\
P_{311}^{\mu\nu\tau} &= \frac{1}{(D-3)s_{13}}\left(-\frac{D-4}{s_{12}^2}T_{212}^{\mu\nu\tau} - \frac{D-4}{s_{13}s_{23}}T_{332}^{\mu\nu\tau} - \frac{Ds_{23}}{s_{12}s_{13}^2}T_{311}^{\mu\nu\tau} + \frac{D-2}{s_{12}s_{13}}T_{312}^{\mu\nu\tau}\right)\,,\\
P_{312}^{\mu\nu\tau} &= \frac{D-2}{(D-3)s_{12}s_{13}s_{23}}\left(\frac{s_{13}}{s_{12}}T_{212}^{\mu\nu\tau} + \frac{s_{12}}{s_{23}}T_{332}^{\mu\nu\tau} + \frac{s_{23}}{s_{13}}T_{311}^{\mu\nu\tau} + \frac{D}{D-2}T_{312}^{\mu\nu\tau}\right)\,.
\end{aligned} \tag{2.9}$$

JHEP04(2025)060

For the $q\bar{q} \to gH$ amplitude the projectors are [99]:

$$P_1 = \frac{D-2}{2(D-3)s_{12}s_{13}^2} T_1^\dagger - \frac{D-4}{2(D-3)s_{12}s_{13}s_{23}} T_2^\dagger \,,$$
$$P_2 = -\frac{D-4}{2(D-3)s_{12}s_{13}s_{23}} T_1^\dagger + \frac{D-2}{2(D-3)s_{12}s_{23}^2} T_2^\dagger \,, \tag{2.10}$$

where P_1 and P_2 satisfy $\sum_{\text{spins}} P_i M_\rho \epsilon^\rho = F_i$. The six NLO QCD form factors have been computed for the SM case in ref. [21]. We have rescaled the SM form factors by the anomalous coupling c_t. To construct the virtual corrections, we use

$$d\sigma^{\text{V}} \sim 2\Re\left(\mathcal{M}^{\text{V}} \cdot \mathcal{M}^{\text{B},\dagger}\right) = 2\Re\left[\left(\mathcal{M}_f^{\text{2L}} + \mathcal{M}_{Hg}^{\text{1L}}\right) \cdot \left(\mathcal{M}_f^{\text{1L}} + \mathcal{M}_{Hg}^{\text{0L}}\right)^\dagger\right]$$
$$= 2\Re\left[\mathcal{M}_f^{\text{2L}} \cdot \left(\mathcal{M}_f^{\text{1L}} + \mathcal{M}_{Hg}^{\text{0L}}\right)^\dagger + \mathcal{M}_{Hg}^{\text{1L}} \cdot \left(\mathcal{M}_{\text{f}}^{\text{1L}} + \mathcal{M}_{Hg}^{\text{0L}}\right)^\dagger\right] . \tag{2.11}$$

The Born matrix elements arising from the tree level diagrams where the Higgs boson couples to gluons, $\mathcal{M}_{Hg}^{\text{0L}}$, are added to the rescaled SM Born matrix elements at form factor level, using the projectors of eqs. (2.9) and (2.10).

In order to use the 2-loop virtual contribution directly within the `POWHEG-BOX-V2`, we constructed a grid based on the 2000 phase space points at which the 2-loop amplitude has been evaluated, together with an interpolation framework. To this aim we first realise that we can write the amplitude as

$$M(\mu) = M_2 \log(\mu)^2 + M_1 \log(\mu) + M_0. \tag{2.12}$$

Thus, we computed the amplitudes for three values of μ and then solved the equations for M_0, M_1 and M_2. We created a grid for each of the four partonic channels where we stored

$$\beta = \frac{s - m_H^2}{s + m_H^2}, \quad \cos\theta = \frac{t-u}{s-m_H^2}, \quad M_0, M_1, M_2. \tag{2.13}$$

To interpolate the virtual amplitudes for each channel we used a neural network trained on the grid, where we used 30% of the data points as a validation set. For the training of the network we multiplied the coefficients M_0, M_1 and M_2 with $\beta^2(1-\beta)(1-\cos^2\theta)$ and divided by the largest value in the grid. This guarantees that the grid for the neural network training has values in $[-1, 1]$ and is flattened at the phase space boundaries. The architecture of each network is composed of three dense layers with 200, 20 and 20 nodes, respectively. The setup is implemented using `Keras` [100] to produce the models in combination with a modified version of `Keras2cpp` [101] to save them such that they can be loaded from C++. We built a C++ function where, for each channel, the models are loaded. This function is called in the `POWHEG-BOX-V2` to obtain the two-loop virtual amplitude at any given phase space point.

The one-loop amplitudes contributing to the virtual corrections where the Higgs couples to gluons, denoted by $\mathcal{M}_{Hg}^{\text{1L}}$, were computed by GoSam, where the interference $\mathcal{M}_{Hg}^{\text{1L}} \cdot \mathcal{M}_{Hg}^{\text{0L}}$ is straightforward, while we had to slightly modify GoSam in order to compute the $\mathcal{M}_{Hg}^{\text{1L}} \cdot \mathcal{M}_f^{\text{1L}}$ interference.

One full run takes roughly 320 CPU-days, depending on the used hardware. The 320 CPU-days refer to a cluster which consists of Intel Xeon Gold 6230 processors with a frequency of 2.1 GHz. It is also worth mentioning that using either $c_t = 0$ or $c_g = 0$ can drastically reduce the number of CPU-hours, since this greatly reduces the number of diagrams to be evaluated.

JHEP04(2025)060

Validation. In order to allow for comparisons and cross checks, we implemented both the $m_t \to \infty$ limit as well as the full SM amplitudes at NLO. We checked that taking $m_t \to \infty$ in all diagrams and setting $c_g = 0$ agrees with the SM calculation in the HTL. Furthermore, using the fact that in the HTL the SM reduces to diagrams with an effective Higgs-gluon coupling given by $c_{g,\mathrm{HTL}} = 2/3$, see e.g. [102], and that the HEFT diagrams with a gluon-Higgs coupling reduce to just HTL diagrams without any top-loops, we checked that $c_t \mathcal{M}_f(m_t \to \infty) + c_g \mathcal{M}_{Hg}(m_t \to \infty) = (2/3 c_t + c_g)/c_{g,\mathrm{HTL}} \cdot \mathcal{M}_{\mathrm{HTL}}$. Furthermore, we have validated the interpolation grid that we implemented in the `Powheg` setup by comparing the grid-based result with the result reconstructed directly from the points obtained from the numerical evaluation of the two-loop amplitude. The differences were of the order of the Monte Carlo uncertainties. We also interpolated the Born amplitude of the grid and compared it to the analytical results. Of course, we also checked that taking $c_t = 1$ and $c_g = 0$ agrees with the SM results computed in [21, 24], both at amplitude level and at total cross section level.

3 Numerical results and discussion of anomalous couplings

The results presented in this section were obtained using the PDF4LHC21_40_`pdfas` parton distribution functions [103–106] interfaced to our code via LHAPDF [107], along with the corresponding value for α_s. The masses of the Higgs boson and the top quark have been fixed, as in the virtual amplitude, to $m_H = 125$ GeV, $m_t = 173.055$ GeV, respectively. Their widths have been set to zero. Jets are clustered with the anti-k_T algorithm [108] as implemented in the `fastjet` package [109, 110], with jet radius $R = 0.4$ and a minimum transverse momentum $p_{T,\mathrm{min}}^{\mathrm{jet}} = 30$ GeV. The central scale is given by

$$\mu_0 = H_T/2 = \frac{1}{2}\left(\sqrt{m_H^2 + p_{T,H}^2} + \sum_i |p_{T,i}|\right), \tag{3.1}$$

where the sum is over all final state partons i. The scale uncertainties are estimated by varying the factorisation and renormalisation scales μ_{F} and μ_{R}. The uncertainty bands represent the envelopes of a 3-point scale variation around the central scale.

3.1 Total cross sections and heat maps

The total cross sections obtained with the above settings and for different values of the minimum transverse momentum of the Higgs boson, $p_{T,H}^{\mathrm{min}}$, are given in table 1, where we compare the benchmark point $c_t = 0.9, c_g = 1/15$ to the SM case. We can clearly see that at LO, the difference between BSM and SM is within the corresponding scale uncertainties. At NLO, the scale uncertainties are reduced and the difference becomes noticeable for highly boosted Higgs bosons, but only for a $p_{T,H}$ cut of 800 GeV the difference is clearly outside the scale uncertainties for the considered benchmark point. This shows that already for small deviations from the SM there can be a measurable difference, if the Higgs boson is very highly boosted. Going away further from the SM values for c_g and c_t, the difference would become more pronounced and start at a smaller $p_{T,H}$-cut values. This will become apparent in the discussion of the heat maps shown in figures 4 and 5. In table 2, we show the ratio of the HEFT at the benchmark point $c_t = 0.9$, $c_g = 1/15$ to the SM case, including Monte

JHEP04(2025)060

$p_{T,H}$ cut [GeV]	σ_{cut}(HEFT) [fb]		σ_{cut}(SM) [fb]	
	LO	NLO	LO	NLO
0	$(8^{+3}_{-2}) \cdot 10^3$	$(15^{+0}_{-2}) \cdot 10^3$	$(8^{+3}_{-2}) \cdot 10^3$	$(15^{+0}_{-2}) \cdot 10^3$
50	$(4.5^{+1.8}_{-1.2}) \cdot 10^3$	$(9.1^{+0.1}_{-1.6}) \cdot 10^3$	$(4.5^{+1.8}_{-1.2}) \cdot 10^3$	$(9.1^{+0.0}_{-1.4}) \cdot 10^3$
100	$(1.4^{+0.6}_{-0.4}) \cdot 10^3$	$(2.85^{+0.08}_{-0.5}) \cdot 10^3$	$(1.4^{+0.6}_{-0.4}) \cdot 10^3$	$(2.85^{+0.01}_{-0.5}) \cdot 10^3$
200	$(2.2^{+0.9}_{-0.6}) \cdot 10^2$	$(4.6^{+0.2}_{-0.9}) \cdot 10^2$	$(2.2^{+0.9}_{-0.6}) \cdot 10^2$	$(4.5^{+0.1}_{-0.9}) \cdot 10^2$
400	13^{+6}_{-4}	28^{+2}_{-6}	12^{+5}_{-3}	$25^{+1.6}_{-5}$
600	$1.6^{\,0.7}_{-0.5}$	$3.3^{+0.3}_{-0.7}$	$1.3^{+0.6}_{-0.4}$	$2.7^{+0.2}_{-0.5}$
800	$0.29^{+0.14}_{-0.09}$	$0.60^{+0.07}_{-0.12}$	$0.21^{+0.10}_{-0.06}$	$0.43^{+0.04}_{-0.09}$

Table 1. Total cross sections for different values of $p_{T,H}^{\text{min}}$, The main value is based on the central scale and the uncertainties are obtained from three-point variations around the central scale. The HEFT values are for the benchmark point $c_t = 0.9, c_g = 1/15$. All cross sections have a minimal jet-p_{T} of 30 GeV and thus at LO, the Higgs boson also has a minimal transverse momentum of 30 GeV.

$p_{T,H}$ cut [GeV]	$\sigma_{\text{cut.HEFT}}/\sigma_{\text{cut,SM}}$	
	LO	NLO
0	0.9955 ± 0.0005	1.00 ± 0.04
50	0.9966 ± 0.0006	1.00 ± 0.04
100	1.0002 ± 0.0010	1.00 ± 0.02
200	1.021 ± 0.002	1.01 ± 0.014
400	1.119 ± 0.007	1.10 ± 0.01
600	1.250 ± 0.012	1.22 ± 0.01
800	1.410 ± 0.016	1.37 ± 0.01

Table 2. The ratios of the total cross section for different values of $p_{T,H}^{\text{min}}$ for a HEFT benchmark point with $(c_t, c_g) = (0.9, 1/15)$ relative to the SM cross section. The uncertainties are the error propagated Monte Carlo uncertainties, since the scale uncertainties are correlated in HEFT and SM and thus mostly cancel.

Carlo uncertainties rather than scale uncertainties, as the scale uncertainties are correlated between HEFT and the SM and therefore largely cancel. The ratios clearly demonstrate the behaviour discussed above, i.e. the difference between HEFT and the SM becoming more pronounced for higher values of $p_{T,H}^{\text{min}}$.

The heat maps illustrate the effects of varying c_t and c_g simultaneously, over a parameter range inspired by current bounds from global fits [61, 111]. In figure 4, we show the ratio of the total cross section including anomalous couplings within HEFT to the SM total cross section, both calculated at full NLO. In figure 5, we show how the NLO K-factor is modified by the anomalous couplings.

For the heat maps, we write the total cross section as

$$\sigma = c_t^2 A + 2 c_t c_g B + c_g^2 C\,, \quad \text{with } \sigma_{\text{SM}} = A\,, \quad \sigma_{\text{HTL}} = \left(\frac{2}{3}\right)^2 C_{\text{HTL}}\,, \tag{3.2}$$

JHEP04(2025)060

$p_{T,H}^{\text{cut}}$	A	B	C	C_{HTL}
0	15.0 ± 0.2	21.4 ± 0.5	30.7 ± 0.8	30.7 ± 0.8
50	9.13 ± 0.12	13.1 ± 0.3	18.9 ± 0.5	18.3 ± 0.5
100	2.86 ± 0.02	4.16 ± 0.07	6.17 ± 0.1	6.13 ± 0.09
200	$(4.54 \pm 0.03) \cdot 10^{-1}$	$(7.16 \pm 0.12) \cdot 10^{-1}$	$(11.9 \pm 0.2) \cdot 10^{-1}$	$(11.9 \pm 0.1) \cdot 10^{-1}$
400	$(2.54 \pm 0.01) \cdot 10^{-2}$	$(5.65 \pm 0.08) \cdot 10^{-2}$	$(13.7 \pm 0.1) \cdot 10^{-2}$	$(13.6 \pm 0.1) \cdot 10^{-2}$
600	$(2.73 \pm 0.01) \cdot 10^{-3}$	$(8.37 \pm 0.11) \cdot 10^{-3}$	$(28.9 \pm 0.2) \cdot 10^{-3}$	$(28.6 \pm 0.1) \cdot 10^{-3}$
800	$(4.33 \pm 0.02) \cdot 10^{-4}$	$(17.5 \pm 0.2) \cdot 10^{-4}$	$(80.6 \pm 0.5) \cdot 10^{-4}$	$(80.0 \pm 0.3) \cdot 10^{-4}$

Table 3. Values for A,B and C at NLO in pb at the central scale. The values for the $p_{T,H}$-cut are given in GeV. The uncertainties are the uncertainties of the fit.

where the last relation is based on the fact that, if we denote the effective gluon-Higgs coupling in the HTL of the SM as $c_{g,\text{HTL}}$, then the cross section can be written as $\sigma_{\text{HTL}} = c_{g,\text{HTL}}^2 C_{\text{HTL}}$, with $c_{g,\text{HTL}} = 2/3$ as explained above. Thus it is sufficient to compute the cross section for different values of c_g and c_t and then fit the coefficients A, B and C. For the fit we chose some (c_t, c_g) value pairs across a wide range, even outside the experimental limits, in order to guarantee a good fit.

By construction A, B, C are independent of the variables c_t, c_g and thus

$$\frac{\sigma}{\sigma_{\text{SM}}} = c_t^2 + 2c_t c_g \frac{B}{A} + c_g^2 \frac{C}{A}, \tag{3.3}$$

$$\frac{\sigma_{\text{NLO}}}{\sigma_{\text{LO}}} = \frac{c_t^2 A_{\text{NLO}} + 2c_t c_g B_{\text{NLO}} + c_g^2 C_{\text{NLO}}}{c_t^2 A_{\text{LO}} + 2c_t c_g B_{\text{LO}} + c_g^2 C_{\text{LO}}}. \tag{3.4}$$

Hence it is sufficient to first perform a fit of the LO and NLO coefficients and then use equations (3.3) and (3.4) to compute the K-factors and the ratio to the SM.

In table 3, we list the fitted values for the coefficients using different cuts on the Higgs boson transverse momentum. The corresponding values for variations around the central scale are given in appendix A.

We see that for all cuts the largest coefficient is always the C-coefficient, followed by B and then A. Thus the dominant contributions to the cross sections stem from purely HTL-like diagrams. Note that the reason why for the chosen benchmark point the SM-like diagrams are more important comes from the fact that $c_t = 0.9 \gg c_g = 1/15$, compatible with current constraints. Furthermore, the higher the cut on the transverse momentum of the Higgs boson, the bigger the ratios C/A and B/A become, indicating again that the deviations from the SM start to become more important for high $p_{T,H}$. This stems from the fact that $d\sigma/dp_{T,H} \sim 1/p_{T,H}^a$ scales with $a = 2$ in the full theory and with $a = 1$ in the HTL [112]. We can also see that $C_{\text{HTL}} \approx C$ for all values of the cut. This is to be expected since the HTL in the SM corresponds to the HEFT with $c_g = 2/3$, excluding those top-loops where the top quark only couples to gluons. The latter are suppressed in the HTL since they do not involve a Yukawa coupling. Thus this gives a cross-check of our computations.

As can be seen in figure 4, the difference to the SM cross section can get very pronounced as we deviate further from the interval $c_t + 3/2c_g \in [0.9, 1.1]$. We can also see that the

JHEP04(2025)060

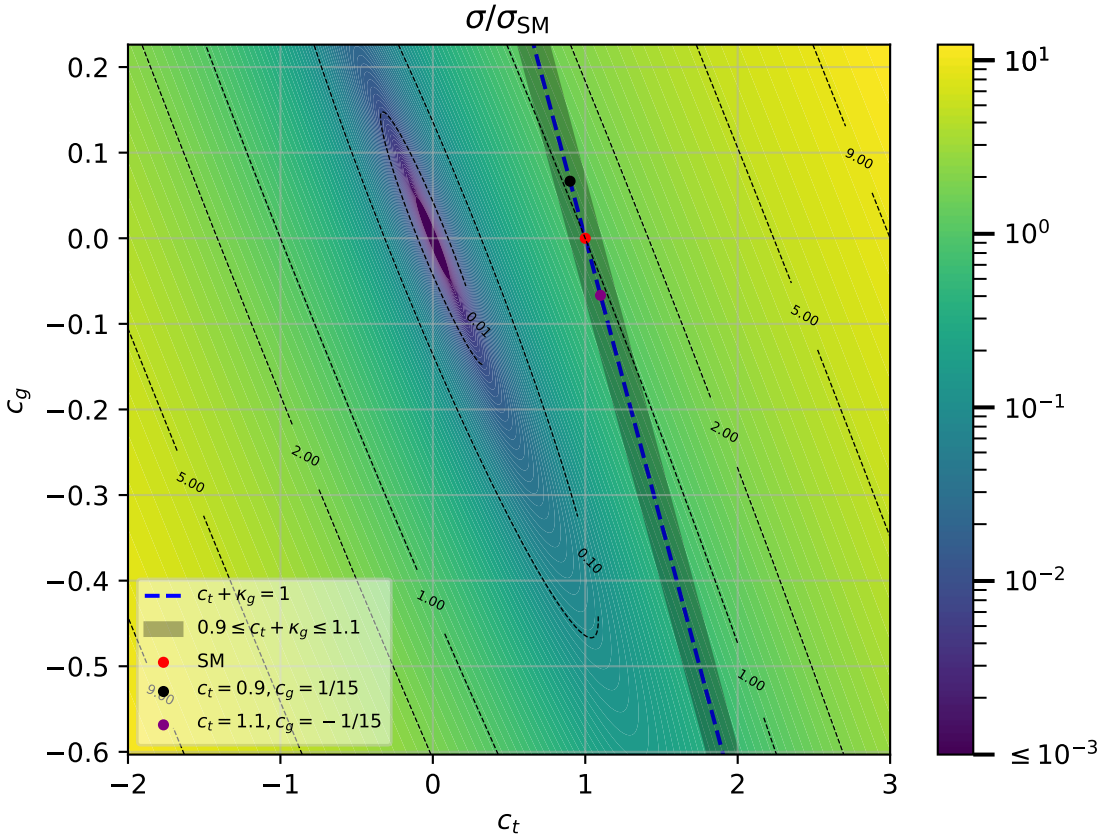

Figure 4. Heat map of the ratio of the HEFT to the SM at the central scale. The colour spectrum is capped at 10^{-3}. The cut on $p_{T,H}$ is 400 GeV.

values of $(c_t, c_g) = (0.9, 1/15)$ and $(c_t, c_g) = (1.1, -1/15)$ are at the boundary to where a difference to the SM starts to become significant. We find that 66.67% of the HEFT points with $c_t + 3/2 c_g \in [0.9, 1.1]$ deviate from the SM result by up to 38%. If we enlarge the interval to $[0.8, 1.2]$, the deviation for 2/3 of the HEFT points in that interval increases to 41%.

In figure 5 we show the ratio of the HEFT K-factors to the SM K-factor. We see that the relative K-factors vary significantly as a function of c_t and c_g.

3.2 Higgs boson transverse momentum distributions

The $p_{T,H}$ distribution with a minimum p_T-cut of 30 GeV on the jet is shown in figure 6, for the SM, the HTL and two HEFT benchmark points. Up to values of $p_{T,H} \approx 300$ GeV there is no significant difference between the considered predictions, but for larger $p_{T,H}$ values the HTL shows large deviations from the SM, whereas the two HEFT parameter points lead to significantly smaller deviations. Thus it is very important to use the SM predictions with full m_t-dependence, otherwise the approximation given by the HTL could mask enhancements in the tail which are in fact BSM effects.

For the two benchmark points we consider, the BSM effects only lie outside the SM NLO QCD scale uncertainty bands for $p_{T,H} \gtrsim 800$ GeV. However, the two benchmark points we chose are quite close to the SM. Choosing larger deformations of the SM case would

JHEP04(2025)060

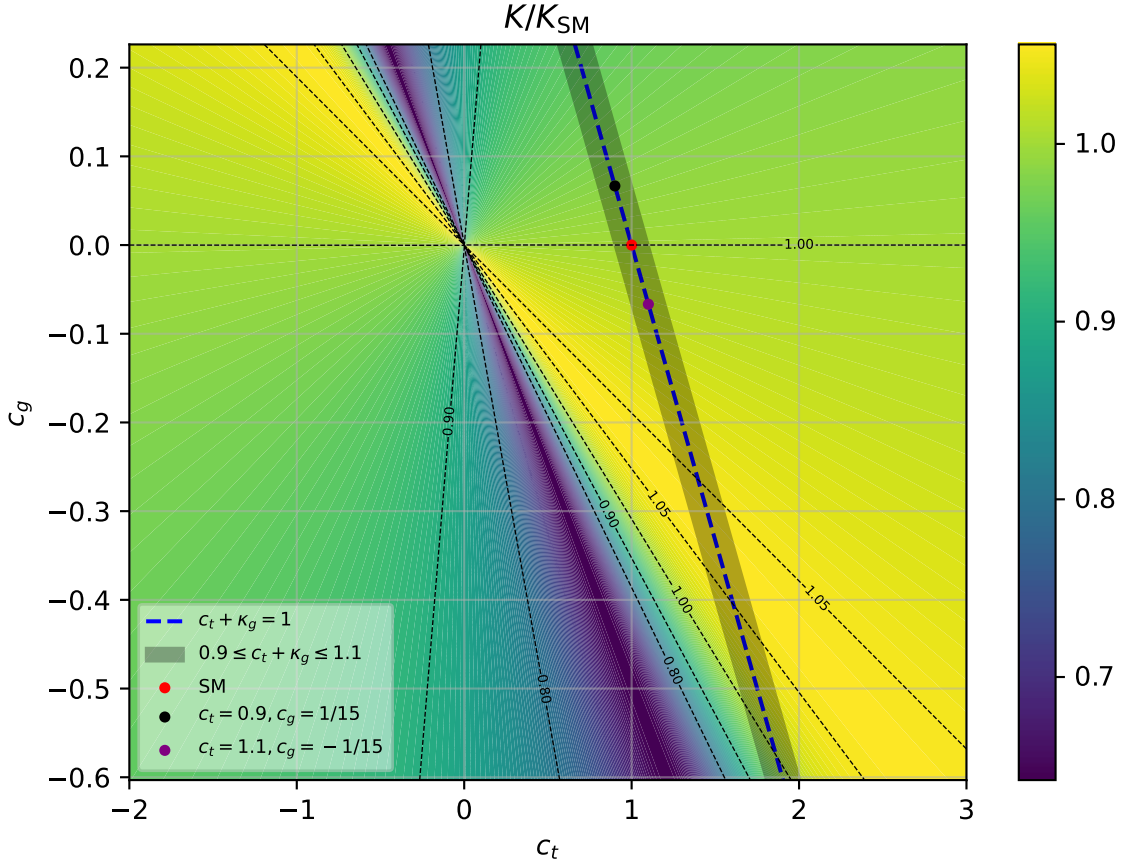

Figure 5. Heat map of the ratio of the NLO K-factors of the HEFT to the SM at the central scale. The cut on $p_{T,H}$ is 400 GeV.

lead to more pronounced effects, visible already at smaller $p_{T,H}$ values. Nonetheless, for very highly boosted Higgs bosons, even small deviations from the SM couplings can lead to characteristic effects. It remains to be investigated whether other SM uncertainties, such as the choice of different top mass renormalisation schemes, can lead to shape distortions that could mask BSM effects. In ref. [31] it was shown that the $p_{T,H}$ distribution with the top quark mass renormalised in the $\overline{\mathrm{MS}}$ scheme falls off faster than in the on-shell (OS) scheme as $p_{T,H}$ increases. However, the ratio OS/$\overline{\mathrm{MS}}$ in the $p_{T,H}$ spectrum stays rather constant for $p_{T,H}$ values between 600 GeVand 1 TeV, while the BSM effects grow much more rapidly with $p_{T,H}$.

Similar considerations hold for the QCD corrections beyond NLO. In ref. [22] the NLO K-factors have been shown to be rather uniform over the whole $p_{T,H}$ spectrum, both in the full SM as well as for the HTL. For the case of the HTL, the ratio between NNLO and NLO also turned out to be rather flat, NNLO increasing the NLO corrections by about 25% for $400\,\mathrm{GeV} \leq p_{T,H} \leq 1\,\mathrm{TeV}$. Thus, a distinctive feature of the anomalous couplings consists in the rapid growth of the shape distortion compared to the SM as $p_{T,H}$ increases.

JHEP04(2025)060

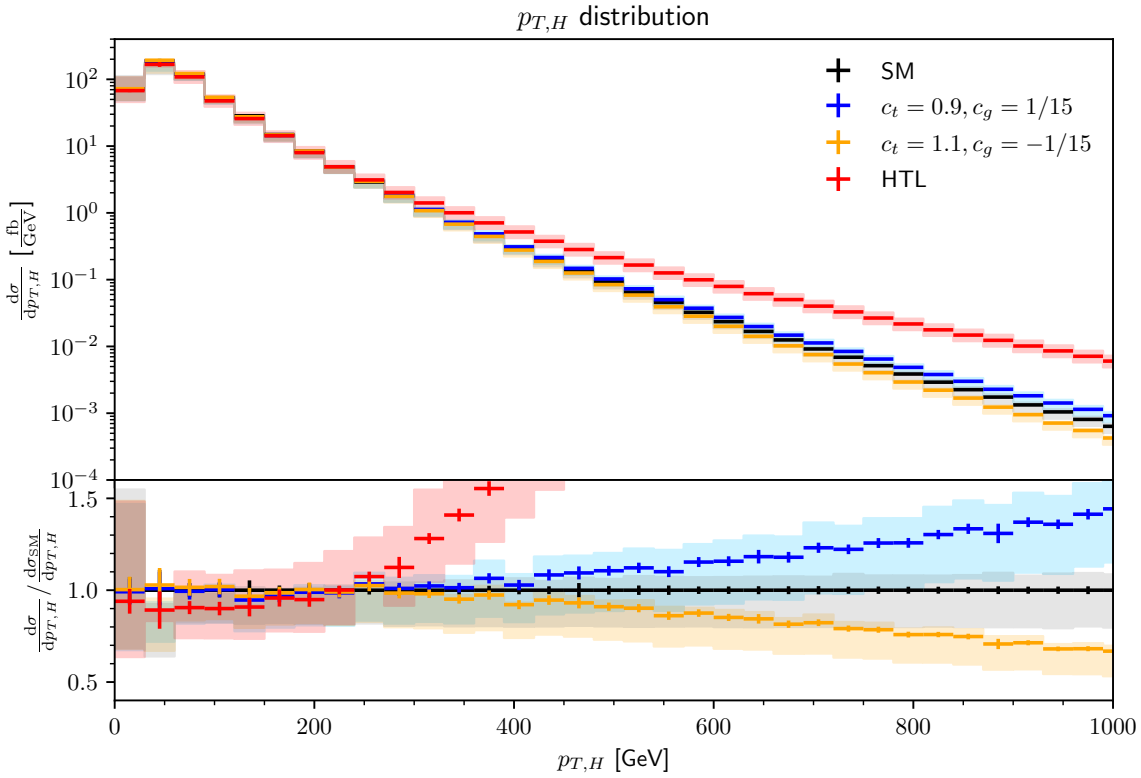

Figure 6. Higgs boson transverse momentum distribution for two HEFT benchmark points, $(c_t, c_g) = (0.9, 1/15)$ and $(c_t, c_g) = (1.1, -1/15)$, compared to the SM case and to the HTL. The bands denote 3-point scale variations around the central scale $\mu_0 = H_T/2$.

4 Conclusions

We have presented results for Higgs boson production in association with one jet, combining full NLO QCD corrections with the leading operators within Higgs Effective Field Theory (HEFT), which can modify the top-Higgs Yukawa coupling and induce an effective Higgs-gluon coupling. We have taken into account constraints arising from the fact that inclusive Higgs production measurements show very good agreement with the SM prediction, assuming that subleading operators, such as the chromomagnetic operator or four-fermion operators, do not play a substantial role. We found that there are combinations of c_t and c_g that reproduce the inclusive Higgs production cross section at the 10% level, while changing the Higgs + jet cross section to an extent that exceeds the scale uncertainties in the highly boosted Higgs regime, i.e. for $p_{T,H}^{\text{min}} \gtrsim 600$ GeV. We also found that the NLO K-factor can vary by more than 30% compared to the SM K-factor within the allowed range of c_t and c_g. Furthermore, we showed that including the full top quark mass dependence is important to avoid that the approximation given by the HTL, leading to an enhancement in the tail of the $p_{T,H}$ distribution, is masking a BSM effect.

A more realistic study should also take into account decays of the Higgs boson as well as prospective statistical uncertainties. Furthermore, it remains to be investigated in more detail whether top mass renormalisation scheme uncertainties could swamp the effects of

JHEP04(2025)060

anomalous couplings even for highly boosted Higgs bosons. On the other hand, a better control of the top mass scheme uncertainties along the lines of ref. [113] seems feasible. In addition, the results presented in ref. [31] for the SM case suggest that the ratio between on-shell and $\overline{\text{MS}}$ renormalisation schemes for the top quark is rather flat for large $p_{T,H}$ values, while the BSM effects grow rapidly with $p_{T,H}$.

Similar considerations hold for QCD corrections beyond NLO, as the K-factors are close to constant in the large $p_{T,H}$ range. This holds for the NLO K-factors both in the HTL and in the full SM, as well as for K_{NNLO} in the HTL [22]. The effects of subleading operators such as the chromomagnetic dipole operator or four-fermion operators also deserve further study, as well as electroweak corrections.

The code is available from the `POWHEG-BOX-V2` website [114] under the process name `Hjet_full_mt`.

Acknowledgments

We would like to thank Matteo Capozi for collaboration at earlier stages of this project. We are also grateful to Gerhard Buchalla, Stephen Jones and Ludovic Scyboz for helpful discussions. This research was supported by the Deutsche Forschungsgemeinschaft (DFG, German Research Foundation) under grant 396021762 — TRR 257. Parts of the computation were carried out on the BwUniCluster2, thus the authors acknowledge support by the state of Baden-Württemberg through bwHPC.

A Coefficients of coupling structures

In this appendix we list the coefficients A, B and C of the anomalous coupling structures, see eq. (3.2), for the three scale choices $\mu_{\text{R}} = \mu_{\text{F}} = \mu_0$, $\mu_{\text{R}} = \mu_{\text{F}} = 2\mu_0$ and $\mu_{\text{R}} = \mu_{\text{F}} = \mu_0/2$. The uncertainties are the uncertainties from the fit.

$p_{T,H}$ cut [GeV]	$\mu_{\text{R}} = \mu_{\text{F}} = \mu_0$	$\mu_{\text{R}} = \mu_{\text{F}} = 2\mu_0$	$\mu_{\text{R}} = \mu_{\text{F}} = 0.5\mu_0$
0	15.0 ± 0.2	12.6 ± 0.13	14.2 ± 0.3
50	9.13 ± 0.12	7.53 ± 0.08	8.98 ± 0.21
100	2.86 ± 0.02	2.35 ± 0.02	2.88 ± 0.04
200	$(4.54 \pm 0.03) \cdot 10^{-1}$	$(3.69 \pm 0.02) \cdot 10^{-1}$	$(4.67 \pm 0.04) \cdot 10^{-1}$
400	$(2.54 \pm 0.01) \cdot 10^{-2}$	$(2.04 \pm 0.01) \cdot 10^{-2}$	$(2.70 \pm 0.02) \cdot 10^{-2}$
600	$(2.73 \pm 0.01) \cdot 10^{-3}$	$(2.19 \pm 0.01) \cdot 10^{-3}$	$(2.94 \pm 0.02) \cdot 10^{-3}$
800	$(4.33 \pm 0.02) \cdot 10^{-4}$	$(3.46 \pm 0.01) \cdot 10^{-4}$	$(4.70 \pm 0.03) \cdot 10^{-4}$

Table 4. Values for A at NLO in pb.

JHEP04(2025)060

$p_{T,H}$ cut [GeV]	$\mu_R = \mu_F = \mu_0$	$\mu_R = \mu_F = 2\mu_0$	$\mu_R = \mu_F = 0.5\mu_0$
0	21.4 ± 0.5	18.0 ± 0.3	22.6 ± 0.8
50	13.1 ± 0.3	10.7 ± 0.2	14.4 ± 0.5
100	4.16 ± 0.07	3.40 ± 0.05	4.62 ± 0.12
200	$(7.16 \pm 0.12) \cdot 10^{-1}$	$(5.81 \pm 0.08) \cdot 10^{-1}$	$(8.05 \pm 0.19) \cdot 10^{-1}$
400	$(5.65 \pm 0.08) \cdot 10^{-2}$	$(4.54 \pm 0.05) \cdot 10^{-2}$	$(6.46 \pm 0.13) \cdot 10^{-2}$
600	$(8.37 \pm 0.11) \cdot 10^{-3}$	$(6.70 \pm 0.07) \cdot 10^{-3}$	$(9.62 \pm 0.18) \cdot 10^{-3}$
800	$(17.5 \pm 0.2) \cdot 10^{-4}$	$(14.0 \pm 1.0) \cdot 10^{-4}$	$(20.1 \pm 0.3) \cdot 10^{-4}$

Table 5. Values for B at NLO in pb.

$p_{T,H}$ cut [GeV]	$\mu_R = \mu_F = \mu_0$	$\mu_R = \mu_F = 2\mu_0$	$\mu_R = \mu_F = 0.5\mu_0$
0	30.7 ± 0.8	25.8 ± 0.5	36.3 ± 1.4
50	18.9 ± 0.5	15.4 ± 0.3	23.0 ± 0.8
100	6.17 ± 0.1	5.03 ± 0.08	7.52 ± 0.2
200	$(11.9 \pm 0.2) \cdot 10^{-1}$	$(9.74 \pm 0.01) \cdot 10^{-1}$	$(14.4 \pm 0.3) \cdot 10^{-1}$
400	$(13.7 \pm 0.1) \cdot 10^{-2}$	$(11.2 \pm 0.1) \cdot 10^{-2}$	$(16.6 \pm 0.2) \cdot 10^{-2}$
600	$(28.9 \pm 0.2) \cdot 10^{-3}$	$(23.4 \pm 0.2) \cdot 10^{-3}$	$(34.9 \pm 0.4) \cdot 10^{-3}$
800	$(80.6 \pm 0.5) \cdot 10^{-4}$	$(65.2 \pm 0.3) \cdot 10^{-4}$	$(97.5 \pm 1.0) \cdot 10^{-4}$

Table 6. Values for C at NLO in pb.

Data Availability Statement. This article has no associated data or the data will not be deposited.

Code Availability Statement. This article has no associated code or the code will not be deposited.

Open Access. This article is distributed under the terms of the Creative Commons Attribution License (CC-BY4.0), which permits any use, distribution and reproduction in any medium, provided the original author(s) and source are credited.

References

[1] R.V. Harlander and T. Neumann, *Probing the nature of the Higgs-gluon coupling*, *Phys. Rev. D* **88** (2013) 074015 [arXiv:1308.2225] [INSPIRE].

[2] A. Azatov and A. Paul, *Probing Higgs couplings with high p_T Higgs production*, *JHEP* **01** (2014) 014 [arXiv:1309.5273] [INSPIRE].

[3] A. Banfi, A. Martin and V. Sanz, *Probing top-partners in Higgs+jets*, *JHEP* **08** (2014) 053 [arXiv:1308.4771] [INSPIRE].

[4] C. Grojean, E. Salvioni, M. Schlaffer and A. Weiler, *Very boosted Higgs in gluon fusion*, *JHEP* **05** (2014) 022 [arXiv:1312.3317] [INSPIRE].

JHEP04(2025)060

[5] M. Schlaffer et al., *Boosted Higgs Shapes*, *Eur. Phys. J. C* **74** (2014) 3120 [arXiv:1405.4295] [INSPIRE].

[6] M. Buschmann et al., *Resolving the Higgs-Gluon Coupling with Jets*, *Phys. Rev. D* **90** (2014) 013010 [arXiv:1405.7651] [INSPIRE].

[7] S. Dawson, I.M. Lewis and M. Zeng, *Effective field theory for Higgs boson plus jet production*, *Phys. Rev. D* **90** (2014) 093007 [arXiv:1409.6299] [INSPIRE].

[8] M. Buschmann et al., *Mass Effects in the Higgs-Gluon Coupling: Boosted vs Off-Shell Production*, *JHEP* **02** (2015) 038 [arXiv:1410.5806] [INSPIRE].

[9] U. Langenegger, M. Spira and I. Strebel, *Testing the Higgs Boson Coupling to Gluons*, arXiv:1507.01373 [INSPIRE].

[10] A. Azatov, C. Grojean, A. Paul and E. Salvioni, *Resolving gluon fusion loops at current and future hadron colliders*, *JHEP* **09** (2016) 123 [arXiv:1608.00977] [INSPIRE].

[11] J.M. Lindert, K. Kudashkin, K. Melnikov and C. Wever, *Higgs bosons with large transverse momentum at the LHC*, *Phys. Lett. B* **782** (2018) 210 [arXiv:1801.08226] [INSPIRE].

[12] J. Alison et al., *Higgs boson potential at colliders: Status and perspectives*, *Rev. Phys.* **5** (2020) 100045 [arXiv:1910.00012] [INSPIRE].

[13] F. Maltoni, E. Vryonidou and C. Zhang, *Higgs production in association with a top-antitop pair in the Standard Model Effective Field Theory at NLO in QCD*, *JHEP* **10** (2016) 123 [arXiv:1607.05330] [INSPIRE].

[14] M. Grazzini, A. Ilnicka, M. Spira and M. Wiesemann, *Modeling BSM effects on the Higgs transverse-momentum spectrum in an EFT approach*, *JHEP* **03** (2017) 115 [arXiv:1612.00283] [INSPIRE].

[15] M. Grazzini, A. Ilnicka and M. Spira, *Higgs boson production at large transverse momentum within the SMEFT: analytical results*, *Eur. Phys. J. C* **78** (2018) 808 [arXiv:1806.08832] [INSPIRE].

[16] M. Battaglia, M. Grazzini, M. Spira and M. Wiesemann, *Sensitivity to BSM effects in the Higgs p_T spectrum within SMEFT*, *JHEP* **11** (2021) 173 [arXiv:2109.02987] [INSPIRE].

[17] F. Maltoni, G. Ventura and E. Vryonidou, *Impact of SMEFT renormalisation group running on Higgs production at the LHC*, *JHEP* **12** (2024) 183 [arXiv:2406.06670] [INSPIRE].

[18] S. Di Noi, R. Gröber and M.K. Mandal, *Two-loop running effects in Higgs physics in Standard Model Effective Field Theory*, *JHEP* **12** (2025) 220 [arXiv:2408.03252] [INSPIRE].

[19] U. Baur and E.W.N. Glover, *Higgs Boson Production at Large Transverse Momentum in Hadronic Collisions*, *Nucl. Phys. B* **339** (1990) 38 [INSPIRE].

[20] K. Melnikov, L. Tancredi and C. Wever, *Two-loop $gg \to Hg$ amplitude mediated by a nearly massless quark*, *JHEP* **11** (2016) 104 [arXiv:1610.03747] [INSPIRE].

[21] S.P. Jones, M. Kerner and G. Luisoni, *Next-to-Leading-Order QCD Corrections to Higgs Boson Plus Jet Production with Full Top-Quark Mass Dependence*, *Phys. Rev. Lett.* **120** (2018) 162001 [*Erratum ibid.* **128** (2022) 059901] [arXiv:1802.00349] [INSPIRE].

[22] K. Becker et al., *Precise predictions for boosted Higgs production*, *SciPost Phys. Core* **7** (2024) 001 [arXiv:2005.07762] [INSPIRE].

[23] T. Neumann, *NLO Higgs+jet production at large transverse momenta including top quark mass effects*, *J. Phys. Comm.* **2** (2018) 095017 [arXiv:1802.02981] [INSPIRE].

JHEP04(2025)060

[24] X. Chen et al., *Top-quark mass effects in H+jet and H+2 jets production*, *JHEP* **03** (2022) 096 [arXiv:2110.06953] [INSPIRE].

[25] M. Czakon, R.V. Harlander, J. Klappert and M. Niggetiedt, *Exact Top-Quark Mass Dependence in Hadronic Higgs Production*, *Phys. Rev. Lett.* **127** (2021) 162002 [*Erratum ibid.* **131** (2023) 179901] [arXiv:2105.04436] [INSPIRE].

[26] M. Niggetiedt and M. Wiesemann, *Higgs-boson production in the full theory at NNLO+PS*, *Phys. Lett. B* **858** (2024) 139043 [arXiv:2407.01354] [INSPIRE].

[27] L. Budge et al., *The one-loop amplitudes for Higgs + 4 partons with full mass effects*, *JHEP* **05** (2020) 079 [arXiv:2002.04018] [INSPIRE].

[28] R. Bonciani et al., *Two-loop planar master integrals for Higgs→ 3 partons with full heavy-quark mass dependence*, *JHEP* **12** (2016) 096 [arXiv:1609.06685] [INSPIRE].

[29] R. Bonciani et al., *Evaluating a family of two-loop non-planar master integrals for Higgs + jet production with full heavy-quark mass dependence*, *JHEP* **01** (2020) 132 [arXiv:1907.13156] [INSPIRE].

[30] H. Frellesvig et al., *The complete set of two-loop master integrals for Higgs + jet production in QCD*, *JHEP* **06** (2020) 093 [arXiv:1911.06308] [INSPIRE].

[31] R. Bonciani et al., *Next-to-leading-order QCD corrections to Higgs production in association with a jet*, *Phys. Lett. B* **843** (2023) 137995 [arXiv:2206.10490] [INSPIRE].

[32] P. Pietrulewicz and M. Stahlhofen, *Two-loop bottom mass effects on the Higgs transverse momentum spectrum in top-induced gluon fusion*, *JHEP* **05** (2023) 175 [arXiv:2302.06623] [INSPIRE].

[33] M. Bonetti, E. Panzer, V.A. Smirnov and L. Tancredi, *Two-loop mixed QCD-EW corrections to $gg \to Hg$*, *JHEP* **11** (2020) 045 [arXiv:2007.09813] [INSPIRE].

[34] M. Becchetti, F. Moriello and A. Schweitzer, *Two-loop amplitude for mixed QCD-EW corrections to $gg \to Hg$*, *JHEP* **04** (2022) 139 [arXiv:2112.07578] [INSPIRE].

[35] M. Bonetti, E. Panzer and L. Tancredi, *Two-loop mixed QCD-EW corrections to $q\bar{q} \to Hg, qg \to Hq$, and $\bar{q}g \to H\bar{q}$*, *JHEP* **06** (2022) 115 [arXiv:2203.17202] [INSPIRE].

[36] M. Becchetti et al., *Planar master integrals for the two-loop light-fermion electroweak corrections to Higgs plus jet production*, *JHEP* **12** (2018) 019 [arXiv:1810.05138] [INSPIRE].

[37] J. Davies, K. Schönwald, M. Steinhauser and H. Zhang, *Next-to-leading order electroweak corrections to $gg \to HH$ and $gg \to gH$ in the large-m_t limit*, *JHEP* **10** (2023) 033 [arXiv:2308.01355] [INSPIRE].

[38] U. Haisch and M. Niggetiedt, *Exact two-loop amplitudes for Higgs plus jet production with a cubic Higgs self-coupling*, *JHEP* **10** (2024) 236 [arXiv:2408.13186] [INSPIRE].

[39] R. Boughezal et al., *Higgs boson production in association with a jet at next-to-next-to-leading order*, *Phys. Rev. Lett.* **115** (2015) 082003 [arXiv:1504.07922] [INSPIRE].

[40] R. Boughezal et al., *Higgs boson production in association with a jet at NNLO using jettiness subtraction*, *Phys. Lett. B* **748** (2015) 5 [arXiv:1505.03893] [INSPIRE].

[41] F. Caola, K. Melnikov and M. Schulze, *Fiducial cross sections for Higgs boson production in association with a jet at next-to-next-to-leading order in QCD*, *Phys. Rev. D* **92** (2015) 074032 [arXiv:1508.02684] [INSPIRE].

[42] X. Chen et al., *NNLO QCD corrections to Higgs boson production at large transverse momentum*, *JHEP* **10** (2016) 066 [arXiv:1607.08817] [INSPIRE].

JHEP04(2025)060

[43] J.M. Campbell, R.K. Ellis and S. Seth, *H + 1 jet production revisited*, *JHEP* **10** (2019) 136 [arXiv:1906.01020] [INSPIRE].

[44] X. Chen, T. Gehrmann, E.W.N. Glover and A. Huss, *Fiducial cross sections for the four-lepton decay mode in Higgs-plus-jet production up to NNLO QCD*, *JHEP* **07** (2019) 052 [arXiv:1905.13738] [INSPIRE].

[45] X. Chen, T. Gehrmann, E.W.N. Glover and A. Huss, *Fiducial cross sections for the lepton-pair-plus-photon decay mode in Higgs production up to NNLO QCD*, *JHEP* **01** (2022) 053 [arXiv:2111.02157] [INSPIRE].

[46] J.R. Andersen et al., *HEJ 2.2: W boson pairs and Higgs boson plus jet production at high energies*, arXiv:2303.15778 [DOI:10.21468/SciPostPhysCodeb.21] [INSPIRE].

[47] J.R. Andersen et al., *High energy resummed predictions for the production of a Higgs boson with at least one jet*, *JHEP* **03** (2023) 001 [arXiv:2210.10671] [INSPIRE].

[48] T. Liu, A.A. Penin and A. Rehman, *Light quark mediated Higgs boson production in association with a jet at the next-to-next-to-leading order and beyond*, *JHEP* **04** (2024) 031 [arXiv:2402.18625] [INSPIRE].

[49] ATLAS collaboration, *Identification of boosted Higgs bosons decaying into b-quark pairs with the ATLAS detector at 13 TeV*, *Eur. Phys. J. C* **79** (2019) 836 [arXiv:1906.11005] [INSPIRE].

[50] ATLAS collaboration, *Constraints on Higgs boson production with large transverse momentum using $H \to b\bar{b}$ decays in the ATLAS detector*, *Phys. Rev. D* **105** (2022) 092003 [arXiv:2111.08340] [INSPIRE].

[51] CMS collaboration, *Inclusive search for highly boosted Higgs bosons decaying to bottom quark-antiquark pairs in proton-proton collisions at $\sqrt{s} = 13$ TeV*, *JHEP* **12** (2020) 085 [arXiv:2006.13251] [INSPIRE].

[52] ATLAS collaboration, *Measurements of the Higgs boson inclusive and differential fiducial cross-sections in the diphoton decay channel with pp collisions at $\sqrt{s} = 13$ TeV with the ATLAS detector*, *JHEP* **08** (2022) 027 [arXiv:2202.00487] [INSPIRE].

[53] CMS collaboration, *Measurement of the Production Cross Section of a Higgs Boson with Large Transverse Momentum in Its Decays to a Pair of τ Leptons in Proton-Proton Collisions at $\sqrt{s} = 13$ TeV*, *Phys. Lett. B* **857** (2024) 138964 [arXiv:2403.20201] [INSPIRE].

[54] F. Feruglio, *The chiral approach to the electroweak interactions*, *Int. J. Mod. Phys. A* **8** (1993) 4937 [hep-ph/9301281] [INSPIRE].

[55] C.P. Burgess, J. Matias and M. Pospelov, *A Higgs or not a Higgs? What to do if you discover a new scalar particle*, *Int. J. Mod. Phys. A* **17** (2002) 1841 [hep-ph/9912459] [INSPIRE].

[56] B. Grinstein and M. Trott, *A Higgs-Higgs bound state due to new physics at a TeV*, *Phys. Rev. D* **76** (2007) 073002 [arXiv:0704.1505] [INSPIRE].

[57] R. Contino et al., *Strong Double Higgs Production at the LHC*, *JHEP* **05** (2010) 089 [arXiv:1002.1011] [INSPIRE].

[58] R. Alonso et al., *The Effective Chiral Lagrangian for a Light Dynamical "Higgs Particle"*, *Phys. Lett. B* **722** (2013) 330 [*Erratum ibid.* **726** (2013) 926] [arXiv:1212.3305] [INSPIRE].

[59] G. Buchalla, O. Catà and C. Krause, *Complete Electroweak Chiral Lagrangian with a Light Higgs at NLO*, *Nucl. Phys. B* **880** (2014) 552 [arXiv:1307.5017] [INSPIRE].

[60] N.P. Hartland et al., *A Monte Carlo global analysis of the Standard Model Effective Field Theory: the top quark sector*, *JHEP* **04** (2019) 100 [arXiv:1901.05965] [INSPIRE].

JHEP04(2025)060

[61] E. Celada et al., *Mapping the SMEFT at high-energy colliders: from LEP and the (HL-)LHC to the FCC-ee*, *JHEP* **09** (2024) 091 [arXiv:2404.12809] [INSPIRE].

[62] W. Buchmuller and D. Wyler, *Effective Lagrangian Analysis of New Interactions and Flavor Conservation*, *Nucl. Phys. B* **268** (1986) 621 [INSPIRE].

[63] B. Grzadkowski, M. Iskrzynski, M. Misiak and J. Rosiek, *Dimension-Six Terms in the Standard Model Lagrangian*, *JHEP* **10** (2010) 085 [arXiv:1008.4884] [INSPIRE].

[64] I. Brivio and M. Trott, *The Standard Model as an Effective Field Theory*, *Phys. Rept.* **793** (2019) 1 [arXiv:1706.08945] [INSPIRE].

[65] G. Isidori, F. Wilsch and D. Wyler, *The standard model effective field theory at work*, *Rev. Mod. Phys.* **96** (2024) 015006 [arXiv:2303.16922] [INSPIRE].

[66] A. Banfi, B.M. Dillon, W. Ketaiam and S. Kvedaraite, *Composite Higgs at high transverse momentum*, *JHEP* **01** (2020) 089 [arXiv:1905.12747] [INSPIRE].

[67] C. Arzt, M.B. Einhorn and J. Wudka, *Patterns of deviation from the standard model*, *Nucl. Phys. B* **433** (1995) 41 [hep-ph/9405214] [INSPIRE].

[68] G. Buchalla, G. Heinrich, C. Müller-Salditt and F. Pandler, *Loop counting matters in SMEFT*, *SciPost Phys.* **15** (2023) 088 [arXiv:2204.11808] [INSPIRE].

[69] G. Buchalla et al., *Higgs boson pair production in non-linear Effective Field Theory with full m_t-dependence at NLO QCD*, *JHEP* **09** (2018) 057 [arXiv:1806.05162] [INSPIRE].

[70] J.R. Ellis, M.K. Gaillard and D.V. Nanopoulos, *A Phenomenological Profile of the Higgs Boson*, *Nucl. Phys. B* **106** (1976) 292 [INSPIRE].

[71] A.I. Vainshtein, V.I. Zakharov and M.A. Shifman, *Higgs Particles*, *Sov. Phys. Usp.* **23** (1980) 429 [INSPIRE].

[72] S. Dawson and H.E. Haber, *Higgs Boson Low-energy Theorems and Their Applications*, *Int. J. Mod. Phys. A* **7** (1992) 107 [INSPIRE].

[73] ATLAS collaboration, *Study of High-Transverse-Momentum Higgs Boson Production in Association with a Vector Boson in the qqbb Final State with the ATLAS Detector*, *Phys. Rev. Lett.* **132** (2024) 131802 [arXiv:2312.07605] [INSPIRE].

[74] GoSam collaboration, *Automated One-Loop Calculations with GoSam*, *Eur. Phys. J. C* **72** (2012) 1889 [arXiv:1111.2034] [INSPIRE].

[75] GoSam collaboration, *GOSAM-2.0: a tool for automated one-loop calculations within the Standard Model and beyond*, *Eur. Phys. J. C* **74** (2014) 3001 [arXiv:1404.7096] [INSPIRE].

[76] C. Degrande et al., *UFO — The Universal FeynRules Output*, *Comput. Phys. Commun.* **183** (2012) 1201 [arXiv:1108.2040] [INSPIRE].

[77] L. Darmé et al., *UFO 2.0: the 'Universal Feynman Output' format*, *Eur. Phys. J. C* **83** (2023) 631 [arXiv:2304.09883] [INSPIRE].

[78] G. Luisoni, P. Nason, C. Oleari and F. Tramontano, *$HW^{\pm}/HZ$ + 0 and 1 jet at NLO with the POWHEG BOX interfaced to GoSam and their merging within MiNLO*, *JHEP* **10** (2013) 083 [arXiv:1306.2542] [INSPIRE].

[79] P. Nason, *A new method for combining NLO QCD with shower Monte Carlo algorithms*, *JHEP* **11** (2004) 040 [hep-ph/0409146] [INSPIRE].

[80] S. Frixione, P. Nason and C. Oleari, *Matching NLO QCD computations with Parton Shower simulations: the POWHEG method*, *JHEP* **11** (2007) 070 [arXiv:0709.2092] [INSPIRE].

JHEP04(2025)060

[81] S. Alioli, P. Nason, C. Oleari and E. Re, *A general framework for implementing NLO calculations in shower Monte Carlo programs: the POWHEG BOX*, *JHEP* **06** (2010) 043 [arXiv:1002.2581] [INSPIRE].

[82] P. Nogueira, *Automatic Feynman Graph Generation*, *J. Comput. Phys.* **105** (1993) 279 [INSPIRE].

[83] J. Kuipers, T. Ueda, J.A.M. Vermaseren and J. Vollinga, *FORM version 4.0*, *Comput. Phys. Commun.* **184** (2013) 1453 [arXiv:1203.6543] [INSPIRE].

[84] G. Cullen, M. Koch-Janusz and T. Reiter, *Spinney: A Form Library for Helicity Spinors*, *Comput. Phys. Commun.* **182** (2011) 2368 [arXiv:1008.0803] [INSPIRE].

[85] P. Mastrolia, G. Ossola, T. Reiter and F. Tramontano, *Scattering AMplitudes from Unitarity-based Reduction Algorithm at the Integrand-level*, *JHEP* **08** (2010) 080 [arXiv:1006.0710] [INSPIRE].

[86] H. van Deurzen, *Associated Higgs Production at NLO with GoSam*, *Acta Phys. Polon. B* **44** (2013) 2223 [INSPIRE].

[87] T. Binoth et al., *Golem95: A numerical program to calculate one-loop tensor integrals with up to six external legs*, *Comput. Phys. Commun.* **180** (2009) 2317 [arXiv:0810.0992] [INSPIRE].

[88] G. Cullen et al., *Golem95C: A library for one-loop integrals with complex masses*, *Comput. Phys. Commun.* **182** (2011) 2276 [arXiv:1101.5595] [INSPIRE].

[89] J.P. Guillet, G. Heinrich and J.F. von Soden-Fraunhofen, *Tools for NLO automation: extension of the golem95C integral library*, *Comput. Phys. Commun.* **185** (2014) 1828 [arXiv:1312.3887] [INSPIRE].

[90] T. Peraro, *Ninja: Automated Integrand Reduction via Laurent Expansion for One-Loop Amplitudes*, *Comput. Phys. Commun.* **185** (2014) 2771 [arXiv:1403.1229] [INSPIRE].

[91] A. van Hameren, *OneLOop: For the evaluation of one-loop scalar functions*, *Comput. Phys. Commun.* **182** (2011) 2427 [arXiv:1007.4716] [INSPIRE].

[92] R.K. Ellis and G. Zanderighi, *Scalar one-loop integrals for QCD*, *JHEP* **02** (2008) 002 [arXiv:0712.1851] [INSPIRE].

[93] A. von Manteuffel and C. Studerus, *Reduze 2 — Distributed Feynman Integral Reduction*, arXiv:1201.4330 [INSPIRE].

[94] S. Borowka et al., *SecDec-3.0: numerical evaluation of multi-scale integrals beyond one loop*, *Comput. Phys. Commun.* **196** (2015) 470 [arXiv:1502.06595] [INSPIRE].

[95] S. Borowka et al., *pySecDec: a toolbox for the numerical evaluation of multi-scale integrals*, *Comput. Phys. Commun.* **222** (2018) 313 [arXiv:1703.09692] [INSPIRE].

[96] G. Heinrich et al., *Expansion by regions with pySecDec*, *Comput. Phys. Commun.* **273** (2022) 108267 [arXiv:2108.10807] [INSPIRE].

[97] G. Heinrich et al., *Numerical scattering amplitudes with pySecDec*, *Comput. Phys. Commun.* **295** (2024) 108956 [arXiv:2305.19768] [INSPIRE].

[98] M. Boggia et al., *The HiggsTools handbook: a beginners guide to decoding the Higgs sector*, *J. Phys. G* **45** (2018) 065004 [arXiv:1711.09875] [INSPIRE].

[99] T. Gehrmann, M. Jaquier, E.W.N. Glover and A. Koukoutsakis, *Two-Loop QCD Corrections to the Helicity Amplitudes for $H \to 3$ partons*, *JHEP* **02** (2012) 056 [arXiv:1112.3554] [INSPIRE].

[100] F. Chollet et al., *Keras*, https://keras.io (2015).

JHEP04(2025)060

[101] G. Perevozchikov et al., *keras2cpp*, https://github.com/gosha20777/keras2cpp.

[102] M. Spira, A. Djouadi, D. Graudenz and P.M. Zerwas, *Higgs boson production at the LHC*, *Nucl. Phys. B* **453** (1995) 17 [hep-ph/9504378] [INSPIRE].

[103] J. Butterworth et al., *PDF4LHC recommendations for LHC Run II*, *J. Phys. G* **43** (2016) 023001 [arXiv:1510.03865] [INSPIRE].

[104] S. Dulat et al., *New parton distribution functions from a global analysis of quantum chromodynamics*, *Phys. Rev. D* **93** (2016) 033006 [arXiv:1506.07443] [INSPIRE].

[105] L.A. Harland-Lang, A.D. Martin, P. Motylinski and R.S. Thorne, *Parton distributions in the LHC era: MMHT 2014 PDFs*, *Eur. Phys. J. C* **75** (2015) 204 [arXiv:1412.3989] [INSPIRE].

[106] NNPDF collaboration, *Parton distributions for the LHC Run II*, *JHEP* **04** (2015) 040 [arXiv:1410.8849] [INSPIRE].

[107] A. Buckley et al., *LHAPDF6: parton density access in the LHC precision era*, *Eur. Phys. J. C* **75** (2015) 132 [arXiv:1412.7420] [INSPIRE].

[108] M. Cacciari, G.P. Salam and G. Soyez, *The anti-k_t jet clustering algorithm*, *JHEP* **04** (2008) 063 [arXiv:0802.1189] [INSPIRE].

[109] M. Cacciari and G.P. Salam, *Dispelling the N^3 myth for the k_t jet-finder*, *Phys. Lett. B* **641** (2006) 57 [hep-ph/0512210] [INSPIRE].

[110] M. Cacciari, G.P. Salam and G. Soyez, *FastJet User Manual*, *Eur. Phys. J. C* **72** (2012) 1896 [arXiv:1111.6097] [INSPIRE].

[111] SMEFiT collaboration, *Combined SMEFT interpretation of Higgs, diboson, and top quark data from the LHC*, *JHEP* **11** (2021) 089 [arXiv:2105.00006] [INSPIRE].

[112] F. Caola et al., *The Higgs transverse momentum spectrum with finite quark masses beyond leading order*, *JHEP* **08** (2016) 150 [arXiv:1606.04100] [INSPIRE].

[113] S. Jaskiewicz, S. Jones, R. Szafron and Y. Ulrich, *The structure of quark mass corrections in the $gg \to HH$ amplitude at high-energy*, arXiv:2501.00587 [INSPIRE].

[114] https://powhegbox.mib.infn.it/.

JHEP04(2025)060